

Analyzing powers for $\pi^\pm p$ elastic scattering between 87 and 263 MeV

G. J. Hofman,^{2,*} G. R. Smith,¹ T. Ambardar,² F. Bonutti,^{3,4} J. T. Brack,⁸ P. Camerini,^{3,4} J. Clark,⁷ P. P. J. Delheij,¹ F. Farzanpay,⁵ L. Felawka,¹ E. Fragiaco,⁴ E. F. Gibson,⁶ J. Graeter,⁹ N. Grion,^{3,4} M. Kermani,² E. L. Mathie,⁵ R. Meier,^{1,†} D. Ottewell,¹ R. J. Peterson,⁸ R. A. Ristinen,⁸ R. Rui,^{3,4} M. E. Sevier,⁷ H. Staudenmaier,¹⁰ R. Tacik,¹ and G. J. Wagner⁹

¹TRIUMF, Vancouver, British Columbia, Canada V6T 2A3

²Department of Physics and Astronomy, University of British Columbia, Vancouver, British Columbia, Canada V6T 2A6

³Istituto Nazionale di Fisica Nucleare, 34127 Trieste, Italy

⁴Dipartimento di Fisica dell'Universita' di Trieste, 34127 Trieste, Italy

⁵University of Regina, Regina, Saskatchewan, Canada S4S 0A2

⁶California State University, Sacramento, California 95819

⁷School of Physics, University of Melbourne, Parkville, Victoria, 3052, Australia

⁸University of Colorado, Boulder, Colorado 80309-0446

⁹Physikalisches Institut, Universität Tübingen, D-72076 Tübingen, Germany

¹⁰University of Karlsruhe, D-76128 Karlsruhe, Germany

(Received 7 July 1998)

Analyzing powers for πp elastic scattering were measured using the CHAOS spectrometer at energies spanning the $\Delta(1232)$ resonance. This work presents π^+ data at the pion kinetic energies 117, 130, 139, 155, 169, 180, 193, 218, 241, and 267 MeV and π^- data at 87, 117, 193, and 241 MeV, covering an angular range of $50^\circ \leq \theta_{c.m.} \leq 180^\circ$ at the higher energies and $90^\circ \leq \theta_{c.m.} \leq 180^\circ$ at the lower energies. Unique features of the spectrometer acceptance were employed to reduce systematic errors. Single-energy phase shift analyses indicate the resulting S_{11} and S_{31} phases favor the results of the SM95 phase shift analysis over that of the older KH80 analysis. [S0556-2813(98)06512-1]

PACS number(s): 13.75.Gx, 24.70.+s, 25.80.Dj

I. INTRODUCTION

For more than a decade the low-energy pion-nucleon database has continued to suffer from discrepancies that hinder the extraction of important and fundamental quantities in particle physics. The determination of the pion-nucleon sigma term ($\Sigma_{\pi N}$), the search for isospin breaking, and the value of the pion-nucleon coupling constant ($f_{\pi NN}$) all require low-energy pion-nucleon scattering data of high accuracy.

The sigma term, an explicit measure of chiral symmetry breaking due to nonzero quark masses, has been of particular interest. Chiral perturbation theory has related it to the baryon mass spectrum and hence to the strange (sea) quark content [$y = 2\langle p|\bar{s}s|p\rangle / (\langle p|\bar{u}u + \bar{d}d|p\rangle)$] of the nucleon wave function. The πN observables can be related to the Σ term using extrapolations of the scattering amplitudes to the subthreshold ($\nu=0$, $t=2\mu^2$) Cheng-Dashen point [1]. Estimates of the Σ term using the widely accepted Karlsruhe (KH80) partial-wave analysis (PWA), using exclusively pre-meson-factory data, by Höhler [2] and Koch and Pietarinen [3] imply $y = 0.2 \pm 0.2$. Newer analyses have both lowered [4] and raised [5] this value. Accurate data in the low-energy regime will constrain future phase shift analyses and reduce

the uncertainties in the extrapolations.

Isospin breaking in the pion-nucleon S -wave amplitude has been inferred in the analysis of low-energy πN data by Gibbs *et al.* [6] and, more recently, by Matsinos [7]. Both analyses, which rely exclusively on data below 100 MeV, report an approximate 7% effect in the difference between elastic and single-charge-exchange real-part S -wave amplitude.

A large set of pion-nucleon differential cross section data exists, but there are discrepancies between the various measurements that far exceed quoted systematic errors. This problem is particularly severe in the π^+ channel below 100 MeV. New differential cross section [$\sigma(\theta)$] data are unlikely to resolve the discrepancies. Spin observables, such as analyzing powers, are the results of an interference between spin-flip (G) and spin-non-flip (H) amplitudes and hence sensitive to smaller, nonresonant partial waves, while the differential and total cross sections are dominated by the resonant P_{33} partial wave.

Moreover, the analyzing power

$$A_y = \frac{\sigma^\uparrow - \sigma^\downarrow}{P^\downarrow \sigma^\uparrow + P^\uparrow \sigma^\downarrow} = \frac{Y^\uparrow/N^\uparrow - Y^\downarrow/N^\downarrow}{P^\downarrow Y^\uparrow/N^\uparrow + P^\uparrow Y^\downarrow/N^\downarrow} = \frac{2 \operatorname{Im}(GH^*)}{(|G|^2 + |H|^2)} \quad (1)$$

is subject to quite different systematic errors. The usual cross section normalization quantities such as solid angle, number of target nuclei, pion decay fraction, and detection efficiencies cancel out, leaving the πp yield (Y^\uparrow), the beam normalization (N^\uparrow), target polarization (P^\downarrow), and back-

*Present address: Department of Physics, CB 446, The University of Colorado, Boulder, CO 80309-0446. Electronic address: gertjan.hofman@colorado.edu

†Present address: Physikalisches Institut, Universität Tübingen, 72076 Tübingen, Germany.

ground as the only sensitive quantities. The $\downarrow\uparrow$ arrows indicate the spin direction of the target protons perpendicular to the pion scattering plane.

There are far fewer analyzing power measurements than measurements of differential cross sections. Before the 1996 π^+ data of Wieser *et al.* [8] (four angles at 68.3 MeV) there was no measurement below 95 MeV. The data of Seviour *et al.* [9] at TRIUMF are the most precise and dominate the database between 98 and 263 MeV for both π^+ and π^- . There are three other data sets that overlap with the energies of this experiment (Alder *et al.* [10], Raue *et al.* [11], Amsler *et al.* [12]) and they will be compared to in Sec. VI

Experiment E560 at TRIUMF used the CHAOS spectrometer [13] to measure πp elastic scattering analyzing powers with the intent of resolving discrepancies in the low-energy pion-nucleon database while simultaneously contributing valuable new data. Part I, described in this paper, acquired data at 10 π^+ energies (117, 130, 139, 155, 169, 180, 193, 218, 240, 267 MeV) and 4 π^- energies (87, 117, 193, 241 MeV). These higher energies, and resulting larger cross sections, were chosen due to the low target polarization achieved in the early phase of the experiment. Moreover, unreliable target polarization measurements forced normalization of these data to those of Seviour *et al.*, a procedure described in more detail in Sec. II C 2. Part II deals with the more recently acquired π^- scattering results at 57, 67, 87, 98, 117, and 139 MeV, and will be reported in a future paper.

II. EXPERIMENTAL APPARATUS

A. Spectrometer

All data were collected with the CHAOS spectrometer and a dedicated spin-polarized target [14] in the M11 pion channel at TRIUMF. A detailed description of the CHAOS spectrometer can be found in Ref. [13] and references therein but those components crucial to E560 are described below.

The spectrometer consisted of low-mass, cylindrical tracking chambers and particle identification counters immersed in a vertical magnetic field provided by a cylindrical dipole magnet with an open geometry. A typical $\pi^- p$ scattering event recorded by the spectrometer is shown in Fig. 1. Radially outwards from the center were the two proportional vertex chambers (WC1, WC2), positioned at 11.5 and 23.3 cm radius, respectively. A drift chamber (WC3 [15]) was positioned at a radius of 34.4 cm. The struck-wire information for WC3 was used in conjunction with that from the two proportional chambers in a second-level trigger [16]. The drift time information was also digitized but was not part of the trigger system. Positioned in the tail of the magnetic field at a radius of 62–66 cm was a vector drift chamber (WC4). This chamber, with 100 cells of 8 anode wires each, vastly improved the particle tracking and momentum resolution. Surrounding the WC4 detector were 2 layers of plastic scintillation counters and an outer layer of lead-glass Cherenkov counters. The counters were arranged in 20 blocks, each 18° wide. The ΔE_1 counters were 3-mm-thick NE110 plastic and faced the target at a radius of 71 cm. Behind each ΔE_1 counter were two adjacent 9° -wide scintillators ΔE_{2l} , ΔE_{2r} made of NE110 plastic 12 mm thick. The outer layer of the glass Cherenkov detectors was not used in this experiment.

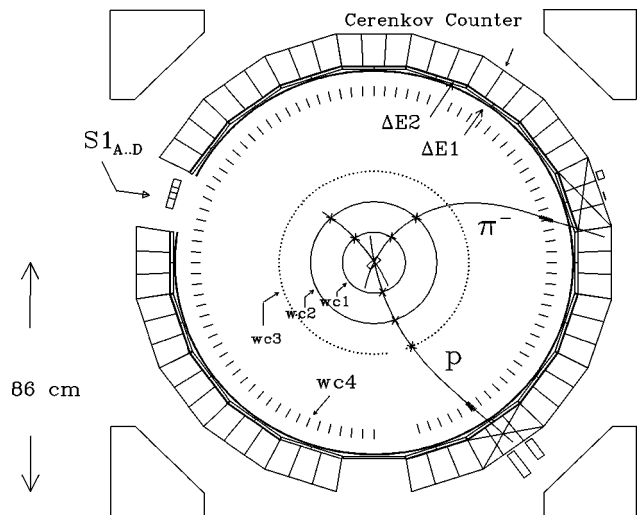


FIG. 1. Typical $\pi^- p$ coincidence event at 140 MeV. The beam pion enters through the four-segment scintillator $S1$, is detected in wire chambers WC1 and WC2, and traced to the target at center. The scattered particles traverse all four wire chambers and stop in the lead-glass detectors. Pulse heights corresponding to the energy loss in the ΔE_1 and ΔE_2 counters, used to mass-identify the particles, are indicated by the rectangular bars.

The counter modules subtended $\pm 7^\circ$ in the vertical direction and defined the out-of-plane acceptance. In the horizontal scattering plane the acceptance was nominally 360° except for a single 18° section removed at the beam entrance.

A four-element scintillation counter hodoscope ($S1$) defined and counted the incident beam, and also provided the time reference for all the readout electronics. It was situated a few cm upstream of WC4, approximately 72 cm from the target. Use of a single hodoscope element to count the beam required normalization corrections discussed in Sec. III. The drift chambers (WC3 and WC4) were deadened in the incoming and outgoing beam regions. However, the incident pions were detected by the proportional chambers WC1 and WC2. Together with the known beam momentum and spectrometer magnetic field, this permitted reconstruction of the incident beam trajectory to the target, which was situated at the center of the spectrometer. Scattered particles were typically detected in all four wire chambers as well as the elements of the scintillation counter blocks.

The magnitudes of the fields for E560 were chosen to provide the greatest curvature for the scattered pions without trapping the lowest-momentum particles. The field was scaled with the incident momentum in order to maintain a similar scattering geometry at all beam energies. For incident pion energies below 170 MeV, this ratio was $P_{in}/B = 171 \text{ MeV}/(\text{cT})$ and at the higher energies it was set at $P_{in}/B = 239 \text{ MeV}/(\text{cT})$.

B. Trigger requirements

The vast majority of the data, including all the $\pi^- p$ data and all but five of the forward angle $\pi^+ p$ data points were collected in coincidence mode in which tracks for both the scattered pion and the recoil proton were identified and fully reconstructed. The requirement that the recoil proton have sufficient energy to exit the target and be tracked reduced the

angular range (a typical cutoff is $\theta_{\pi} > 70^{\circ}_{\text{c.m.}}$ at $T_{\pi} = 139$ MeV) but suppressed all background reactions except for the quasielastic scattering process.

Event filtering was accomplished in CHAOS by three levels of on-line triggering. The first level trigger [17] was based on the multiplicity of hits in the ΔE_1 and ΔE_2 counters. The second level trigger [16] analyzed the data from WC1, WC2, and WC3 and made decisions based on the possible number of scattered tracks, their polarity, momentum, and distance of closest approach to the center of CHAOS. The third level was a software trigger running on a VME data acquisition computer.

Each of the 19 counter blocks was potentially an active contributor to the hit multiplicity that formed the output of the first level trigger. The trigger multiplicity was set to require at least two tracks (“coincidence” trigger) except for some data acquired at 117 and 139 MeV π^+p where only a single hit was required. Since the low-energy recoil protons stopped in the ΔE_1 counters, hits in the ΔE_2 counters were not demanded in the trigger. Note that the first level trigger logic could not distinguish the geometric location of the hits, a task which was left to the third-level software trigger. For all CHAOS experiments one of the 18° blocks was removed to allow unhindered beam entry into the spectrometer and, similarly, one block was usually removed at the beam exit. For the π^+p reaction, the consequence of removing the beam exit block would have been that the forward (high-kinetic-energy) recoil protons would not be detected and could not have contributed to the coincidence trigger, exactly in the kinematic region where they were most likely to escape the target. A special counter block, consisting only of the ΔE_1 and ΔE_2 counters, was placed at the beam exit. The ΔE_1 counter was used as a veto counter for unscattered beam pions but at the same time, by setting an appropriate pulse height threshold, could contribute to the trigger multiplicity if struck by a recoil proton.

A passed first-level trigger signal started the second-level trigger, and provided the gate for the digitization systems and the stop for the drift chamber timing signals. The second-level trigger performed a triple computational loop the trigger over all struck-wire numbers from the three inner wire chambers (WC1–WC3). This experiment required the trigger logic to find a single scattered track of positive polarity for π^+p , and of either positive or negative polarity for π^-p . In addition the tracks were required to have a distance of closest approach to the target of less than 5 cm. Requiring the presence of a second track in the second-level trigger would have suppressed events where either of the scattered particles passed through deadened sections of WC3. In addition it would have increased the sensitivity to chamber efficiency fluctuations (1–2% expected from slight changes in chamber gas composition and atmospheric pressure, neither of which were monitored), since all chamber hits are then required at all times. The off-line particle tracking allows for one missing hit and hence the pion yield was not affected by these small changes.

Further second-level trigger criteria included valid hits in the incoming beam regions of WC1 and WC2. This condition efficiently eliminated events with muons from in-flight pion decay that entered CHAOS at the wrong angle with respect to the beam axis.

The final, third-level trigger stage consisted of software requirements in the VME data acquisition computer, and performed event rejection based on a partial readout of the data. It required that the time of flight of particles from the pion production target to S1 correspond to pions, reducing electron and muon contamination. When the first-level trigger was set to coincidence mode, the third-level trigger also required that the hits in the ΔE_1 counters corresponded to the expected kinematics from an elastic πp event.

Typical coincidence trigger rates (139 MeV π^+) were 2000 Hz from the first level, reduced to 400 Hz by the second-level trigger, and finally to 140 Hz accepted by the third-level software trigger.

C. Polarized target

A spin-polarized target [14] operating in frozen spin mode was designed specifically for use with the CHAOS spectrometer. The target cell consisted of a $(30 \times 25 \times 5)$ mm³ ($W \times H \times T$) copper vessel of 250 μm wall thickness. The target material was a mixture of butanol ($\text{C}_4\text{H}_9\text{OH}$) and EHBA (sodium bis [2-ethyl-2-hydroxybutyrate(2-)] oxochromate (V) Monohydrate Cr (V)). The relative concentrations were 5×10^{19} molecules of EHBA to 1 cm³ of butanol. Water was added to the mixture in a 1:20 ratio by volume. The liquid target material was pumped into the target cell using a syringe and frozen into a solid slab at liquid nitrogen temperature.

To obtain sufficiently long polarization relaxation times (> 400 h) the target temperature must be kept below 100 mK. This was achieved using a standard dilution refrigerator technique. The mixing chamber surrounded the cell, with the $^4\text{He}/^3\text{He}$ interface immediately above the target cell. The refrigerator cooled the cell from 1.2 K to the operating temperature of 60–70 mK.

1. Polarization procedure

The CHAOS magnetic field served as the polarization holding field during the data acquisition but it did not have the required strength or the 1 in 10^4 homogeneity to serve as a polarizing magnet. A separate superconducting solenoid (PS), outside of CHAOS, provided the necessary homogeneous 2.5 T field for polarization. A third magnet, the holding coil (HC), also superconducting, was situated immediately above the butanol target cell inside the cryostat and was required during transit of the cryostat from the polarizing magnet to the center of CHAOS.

The polarization procedure then consisted of the following steps. The target was dynamically polarized in the PS, and the final polarization achieved was measured as described below. The PS was ramped from 2.5 T to ~ 0.3 T. The HC was then energized to provide ~ 0.3 T in its fringe field, and the target was raised about 50 cm until it cleared the top of the PS. The PS was then rolled clear and the target was lowered 1.4 m through the open 16-cm-diam bore of the CHAOS magnet until it reached beam height. The CHAOS field at this point was 0.3 T at the center. Then the HC was ramped off and the CHAOS field was ramped up to the field required for the πp scattering measurements, usually in excess of 1 T. After completing the scattering measurements slated for that polarization, the same sequence was reversed.

The average loss of polarization during this transportation sequence was determined from target NMR measurements before and after data acquisition. Repeated trial round trips, in which the target was inserted and immediately extracted from the CHAOS magnet, showed that typical transit losses were 3–5 % of the original polarization. Polarization decay times at the operating field of CHAOS were always in excess of 400 h, resulting in negligible decay during the data taking.

2. NMR measurements

The magnitude of target polarization was initially determined from measurements of the proton NMR signal. The NMR coil was a single copper wire loop (1 mm diameter and coated with Teflon) permanently embedded inside the target cell. It was part of an external two-arm Q-meter circuit, driven at the proton Larmor frequency (107.0 MHz at $B = 2.508$ T). The signal from the compensating arm was subtracted from that of the NMR arm containing the embedded coil, to increase the signal-to-noise ratio. The combined signal was amplified, fed into a phase sensitive detector, and digitized. Spin-spin interactions broaden the Zeeman absorption lines. Thus the resonance frequency was scanned (in 512 steps of 2 kHz) around the Larmor frequency. The integrated NMR signal area is proportional to the target polarization.

The standard technique to obtain an absolute calibration of the target polarization is to compare the integrated dynamic NMR signal area with the NMR signal area obtained at some equilibrium temperature, where the polarization at the field H and temperature T is determined by the Boltzmann distribution. These thermal equilibrium (TE) signals were recorded weekly. The field strength was determined from the NMR center frequency and the temperature (≈ 1.1 K) from the ^3He vapor pressure measured directly above the target cell.

To obtain background signals for the NMR measurement, the magnetic field was lowered by 3% to shift the Larmor frequency away from the resonance. Background signals were acquired over the same frequency range over which the real NMR signals were measured. The magnetic field was readjusted to 2.508 T and the foreground signal measured over a frequency range wide enough to include off-resonance regions. The signal areas were then determined using the expression

$$A_{\text{therm}} = \sum_{i=1}^{512} S_i - (\alpha + \beta f_i) B_i + \gamma, \quad (2)$$

where S_i is the foreground signal at frequency f_i , B_i is the background signal, and α, β, γ are fitting parameters determined by minimizing the appropriate χ^2 over regions away from the resonance peak.

Comparison of the CHAOS data acquired in the initial stages of the experiment to the analyzing powers obtained by Sevier *et al.* [9] at 139 MeV π^+ showed that the target polarizations obtained using the NMR thermal equilibrium signals were unreliable. The indicated polarizations were only 30–35 %, far below the 50–60 % expected from the TE calibration. Although calibration using TE NMR signals is usually considered reliable, during this experiment the TE NMR signals were of poor quality, consisted of two peaks instead

of one, had a poor signal-to-noise ratio, and the NMR system was observed to be unstable at the TE level. The dynamic NMR signals, which are two orders of magnitude larger, were adequate. It was therefore decided to deduce the target polarization (see the next section) by comparison of our π^+ data at 139 MeV to the statistically highly precise A_y data of Sevier *et al.* at the same energy. That paper reports a systematic error in the polarization of 1.6%.

The fit of our data to that of Sevier *et al.* only determined the average of our spin-up and spin-down polarization. Since the magnitudes of the polarizations were comparable, the fitted polarization (\bar{P}) is equal to $\frac{1}{2}(P\uparrow + P\downarrow)$ to first order, and the individual polarizations could be extracted using the integrated areas of the dynamic NMR signals. As discussed in the next section, the individual polarization values were only essential for the π^- data.

III. MEASUREMENT PROCEDURE

Two novel measurement techniques were used in this experiment. The normal procedure in analyzing power measurements is to perform a sequence of target spin flips at each incident pion energy. Only after each spin-flip sequence is the beam energy varied, in order to avoid potential instrumental asymmetries. To reduce the systematic error from the uncertainty in the target polarization, this experiment varied the beam energy while maintaining the target polarization. For π^+ , every such set of pion incident energies began and ended with a measurement at 139 MeV π^+ to determine the absolute polarization and its decay rate by comparison with the data of Sevier *et al.* This resulted in two sets of analyzing powers at five or six energies that have *no independent* systematic polarization error but only one overall normalization correction due to the uncertainties in the data of Sevier *et al.* In principle, no target NMR signals are required. Most data were measured twice at each pion energy in order to allow consistency checks.

The spectrometer magnetic field direction must be reversed when changing from π^+ to π^- . Thus the π^- data set could not start and end with 139 MeV π^+ measurements. However, four independent sets of π^+p polarization data at 139 MeV were acquired immediately prior to and with the

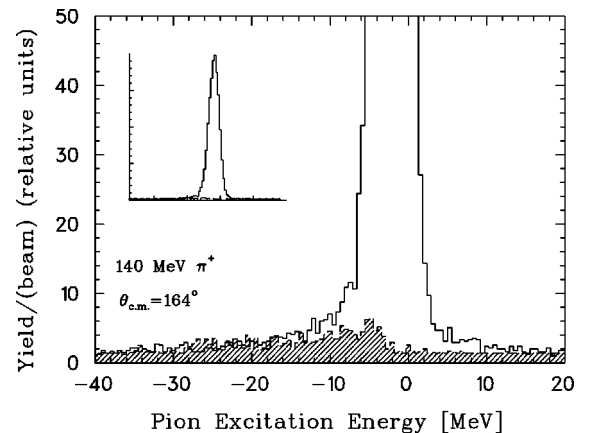


FIG. 2. Coincidence trigger pion excitation spectra at 140 MeV π^+ , $\theta_{\text{lab}}^{\pi} = 160 \pm 5^\circ$. The summed background yields (carbon, helium, and empty target cell) are superimposed (hatched).

same target sample as the π^-p data. These provided a reliable relationship between measured dynamic NMR areas (A) and the calculated target polarizations (P). This calibration [$P = (2.623 \pm 0.021) \times 10^{-3} \% \times A$] was subsequently used to evaluate the target polarization for the π^-p data runs.

The standard procedure of flipping target polarization while maintaining the beam tune parameters serves to minimize possible systematic errors in beam counting. The second novel and powerful technique in this experiment was to use the the 360° acceptance of CHAOS to avoid beam counting altogether. The symmetry inherent to the scattering from a spin-1/2 particle polarized perpendicular to the scattering plane requires that

$$A_y(\theta) = -A_y(-\theta). \quad (3)$$

Since the CHAOS spectrometer measures most angles in the left hemisphere simultaneously with those in the right hemisphere, Eq. (3) can be used to verify or correct the relative normalization of the spin-up and -down scattering yield. Let α be the measured ratio of the beam counts N_\uparrow to N_\downarrow . The analyzing power can then be written as

$$A_y = \frac{Y_\uparrow - \alpha Y_\downarrow}{P_\downarrow Y_\uparrow + \alpha P_\uparrow Y_\downarrow}, \quad (4)$$

where α can be corrected by minimizing

$$\chi^2 = \sum_i^{n/2} \frac{[A_y(\theta_i) + A_y(-\theta_i)]^2}{\delta A_y(\theta_i)^2 + \delta A_y(-\theta_i)^2}$$

or

$$\chi^2 = \sum_i^n \frac{[A_y(\theta_i) - A_p(\theta_i)]^2}{\delta A_y(\theta_i)^2}, \quad (5)$$

where n is the total number of data points (angles). The second expression, which uses some antisymmetric function A_p , such as an existing phase shift solution, is more convenient because it does not require all data at measured angles θ to have counterparts at $-\theta$. This solves problems arising from gaps in the angular distribution between 235° and 255°, which are due to the removal of the scintillator block

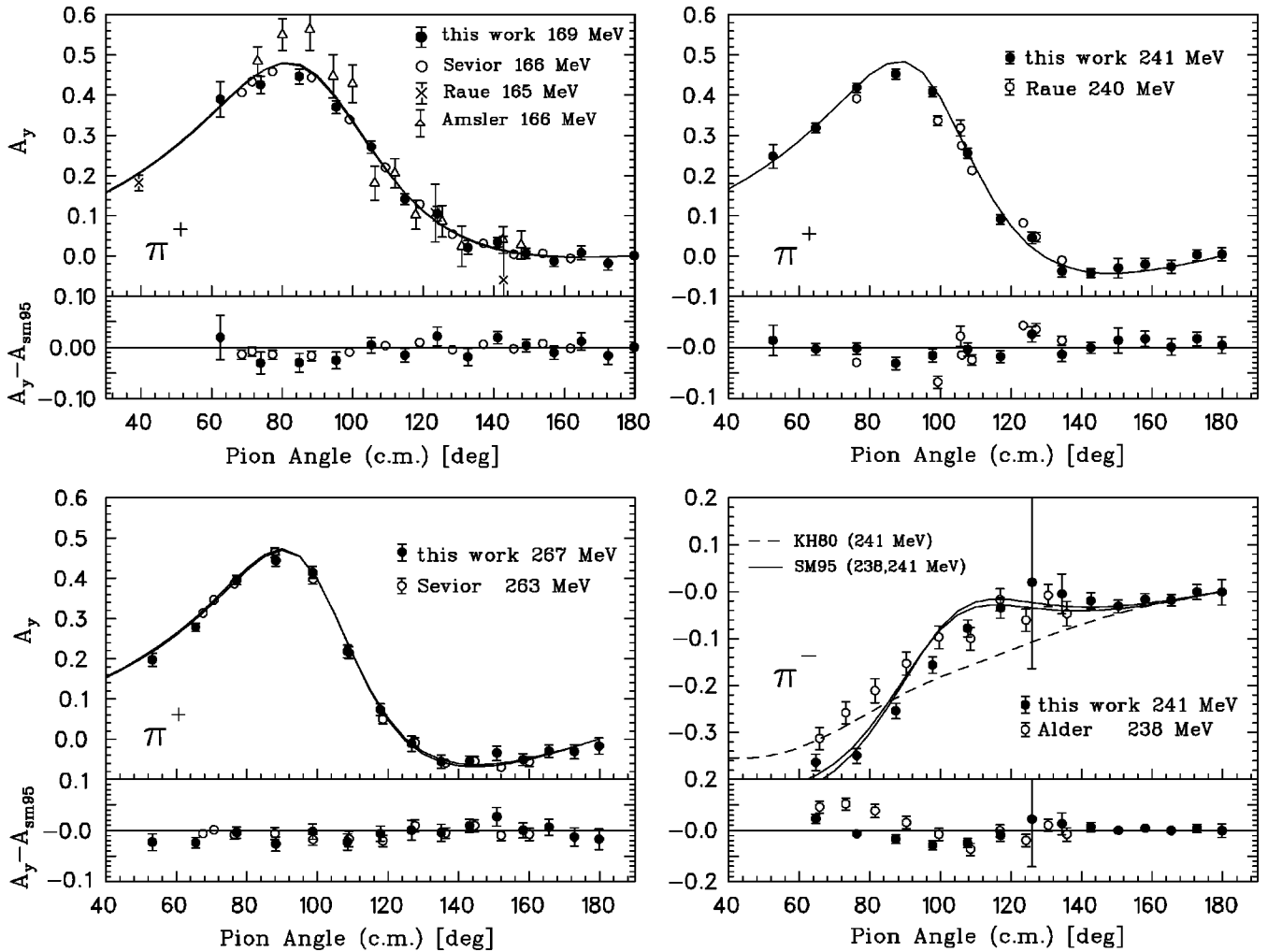


FIG. 3. The new analyzing powers compared to existing data sets for 169, 240, and 263 MeV π^+ and at 241 MeV π^- (Alder *et al.* [10], Raue *et al.* [11], Amsler *et al.* [12], Seviior *et al.* [9]). The lower graphs are the experimental analyzing powers subtracted from the SM95 predictions. Some of the other data sets are at slightly different incident pion energy. To illustrate the small dependence of the analyzing power on the incident beam energy, the SM95 solutions (solid lines) are overlaid for the energies corresponding to the various data sets. The dashed line on the 241 MeV π^- figure is the KH80 solution.

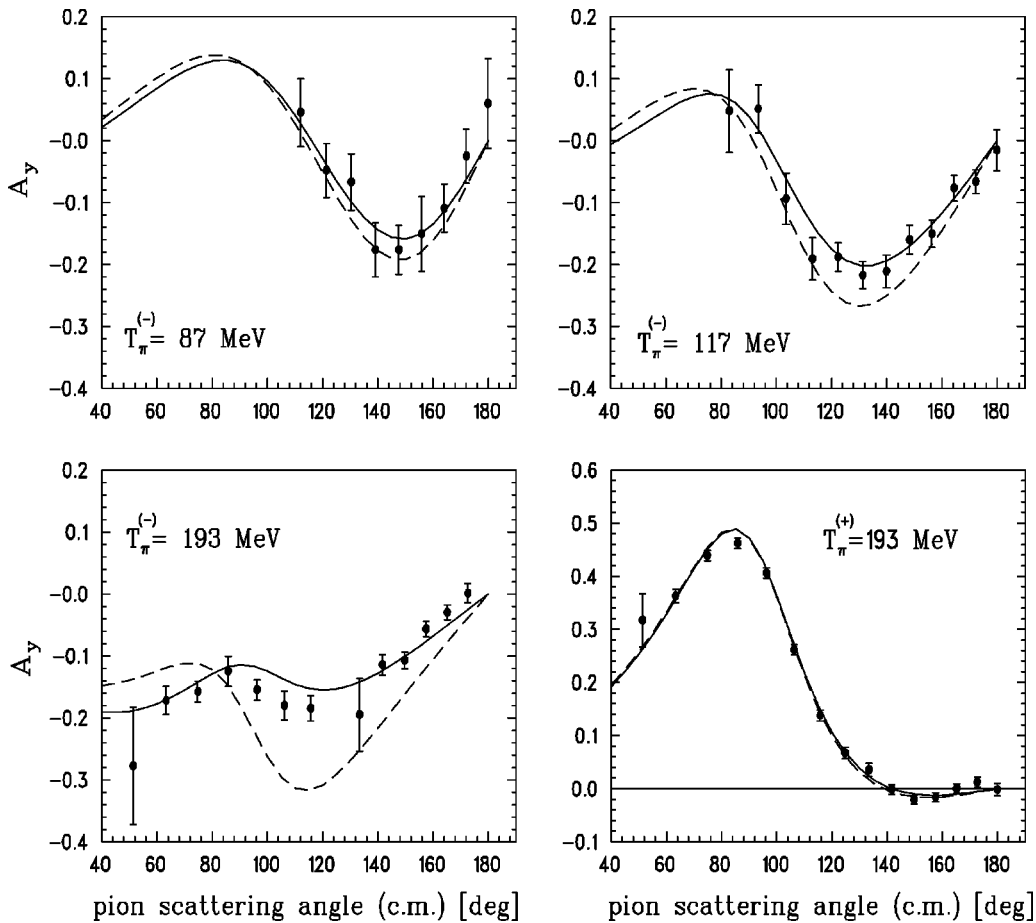


FIG. 4. The analyzing powers for 87, 117, and 193 MeV π^- and 193 MeV π^+ . The solid line is the SM95 solution and the dashed line is the KH80 solution.

in the incoming beam region. The sensitivity of the results to the specific choice of antisymmetric function was investigated and none was found.

Typical values for the correction to α are 0.97–1.03 with a statistical error of less than 0.3%. It should be noted from Eq. (4) that when the average of the analyzing powers at θ and $-\theta$ is calculated, there is only a weak dependence on α (or, equivalently, on the beam normalization) and in fact none if the statistical errors of the data at the two complementary angles were equal. Therefore the final analyzing powers have negligible beam normalization errors.

The absence of absolute beam normalization as one of the two dominant sources of systematic errors is a unique property of the analyzing power data measured with CHAOS. The technique of varying the beam energy while leaving the target polarized was possible only because there was no need to reposition the beam accurately after each channel energy change.

IV. BACKGROUND SUBTRACTION

Background reactions are expected from the carbon and oxygen in the butanol target, the $^4\text{He}/^3\text{He}$ coolant mixture, the target cell, and cryostat windows. The vast majority of the data presented here were acquired in coincidence mode, in which the recoil proton is always detected. This trigger reduced the angular coverage but eliminated elastic scattering from $Z > 1$ nuclei and all reactions that do not produce a

pion and proton in the final state. Additional kinematic cuts on the proton momentum and scattering angle and on the pion momentum as well as on the reaction vertex strongly suppress the background from the (three-body) quasielastic scattering processes. These processes scale approximately with the free πp cross section.

Coincidence data background yields were explicitly measured using targets consisting of a 2.7 ± 0.1 mm graphite slab (C), the target without butanol but with helium coolant (He), and the target completely empty of butanol or coolant (MT), at energies of 87 MeV π^- , 139 MeV π^+ , and 240 MeV π^\pm (carbon only). Figure 2 shows the pion excitation energy histogram at $E_\pi = 139.5$ MeV and $\theta_\pi = 160^\circ$ (coincidence trigger), with the summed backgrounds superimposed. The excitation energy is defined as $E_{\text{obs}} - E_{\pi p}$, the difference between the observed kinetic energy and that predicted using the pion scattering angle and πp kinematics. The target background fractions were deduced from elastic scattering peaks in singles trigger runs and the total background (MT+He+C) matches the tails of the distributions quite well. The integrated background yield under the πp peak is negligible. Similar spectra were obtained at 87 and 240 MeV.

Results for the two most forward angles at 117 and 139 MeV π^+ were only obtained with a singles trigger. For these cases only, the measured C, He, and MT backgrounds were explicitly subtracted after fitting them to the foreground yield

TABLE I. Measured analyzing power at 117 and 139 MeV π^+ and 87 and 117 π^- . These data were collected in the conventional mode and may be independently floated within the systematic error of 3%.

θ_c^π	$A_y(\theta) \pm \delta A_y(\text{stat})$	θ_c^π	$A_y(\theta) \pm \delta A_y(\text{stat})$
116.8 MeV π^+		139.5 MeV π^+	
49.13	0.278±0.022	37.68	0.231±0.029
60.78	0.380±0.020	49.79	0.290±0.021
72.05	0.431±0.022	61.53	0.338±0.024
82.92	0.435±0.019	72.87	0.472±0.033
93.38	0.306±0.020	83.78	0.457±0.024
103.42	0.244±0.018	94.24	0.351±0.020
113.06	0.164±0.016	104.26	0.277±0.019
122.32	0.081±0.012	113.85	0.184±0.016
131.24	0.079±0.012	123.05	0.097±0.011
139.85	0.035±0.015	131.88	0.050±0.010
148.20	0.035±0.015	140.40	0.033±0.011
156.34	-0.007±0.013	148.65	0.019±0.009
164.31	0.012±0.015	156.68	0.014±0.008
172.18	-0.004±0.017	164.55	-0.005±0.008
180.00	0.048±0.031	172.30	0.004±0.009
		180.00	0.020±0.019
86.8 MeV π^-		116.8 MeV π^-	
92.19	0.215±0.166	82.92	0.048±0.067
102.26	0.229±0.082	93.38	0.051±0.039
111.96	0.045±0.055	103.42	-0.094±0.041
121.31	-0.048±0.044	113.06	-0.191±0.034
130.33	-0.067±0.046	122.32	-0.188±0.024
139.07	-0.176±0.044	131.24	-0.217±0.022
147.56	-0.177±0.040	139.85	-0.211±0.027
155.85	-0.151±0.060	148.20	-0.160±0.023
163.99	-0.109±0.039	156.34	-0.151±0.022
172.02	-0.025±0.044	164.31	-0.077±0.021
180.00	0.060±0.072	172.18	-0.066±0.019
		180.00	-0.015±0.033

observed in the scattered pion excitation energy spectra. For this as well as for the coincidence data, fixed 10° -wide bins in the pion scattering angle were always used.

The singles trigger data included angles at which the recoil proton was detected. This allows a comparison of the analyzing power extracted using background subtraction and that extracted by off-line coincidence requirements. It showed that, within the statistical error introduced by background subtraction, the two analyses were equivalent. This also affirmed the assumption that the kinematics cuts made in the coincidence analysis mode effectively eliminated the quasielastic background.

V. RESULTS

A selection of the results is shown in Figs. 3 and 4. The π^+ data not shown are very similar in shape and statistical accuracy to the data at 193 and 267 MeV. All results are tabulated in Tables I–IV and are grouped according to the method in which they were acquired. Table I contains data acquired in the conventional mode in which the target was repolarized in between measurements. Each set in this table

TABLE II. Measured analyzing power between 117 and 169 MeV π^+ . This is the first group of data taken at the same target polarization. These data should not be floated independently. The overall systematic error is 3%.

θ_c^π	$A_y(\theta) \pm \delta A_y(\text{stat})$	θ_c^π	$A_y(\theta) \pm \delta A_y(\text{stat})$
116.8 MeV π^+		130.0 MeV π^+	
82.92	0.438±0.035	83.42	0.431±0.021
93.38	0.331±0.023	93.88	0.325±0.016
103.42	0.244±0.025	103.91	0.238±0.019
113.06	0.149±0.019	113.52	0.161±0.015
122.32	0.085±0.015	122.74	0.072±0.012
131.24	0.054±0.012	131.61	0.055±0.010
139.85	0.015±0.016	140.17	0.026±0.009
148.20	0.041±0.011	148.46	0.035±0.009
156.34	0.020±0.010	156.54	0.002±0.010
164.31	0.009±0.014	164.45	0.004±0.010
172.18	-0.004±0.014	172.25	-0.002±0.016
180.00	0.015±0.017	180.00	-0.024±0.023
139.5 MeV π^+		155.0 MeV π^+	
72.86	0.460±0.024	73.43	0.454±0.022
83.76	0.449±0.012	84.36	0.467±0.014
94.22	0.348±0.010	94.82	0.385±0.013
104.24	0.246±0.012	104.82	0.289±0.018
113.83	0.162±0.010	114.38	0.148±0.013
123.03	0.096±0.008	123.53	0.081±0.011
131.87	0.052±0.007	132.31	0.047±0.009
140.39	0.043±0.006	140.77	0.037±0.008
148.64	0.022±0.006	148.95	0.020±0.008
156.67	0.011±0.007	156.91	0.004±0.008
164.54	0.005±0.007	164.70	0.016±0.010
172.30	-0.010±0.007	172.38	-0.013±0.009
180.00	0.014±0.016	180.00	0.009±0.013
169.0 MeV π^+		169.0 MeV π^+ (continued)	
62.53	0.296±0.055	132.72	0.026±0.010
73.96	0.479±0.020	141.11	0.000±0.010
84.90	0.477±0.015	149.23	0.005±0.009
95.37	0.376±0.015	157.12	-0.002±0.014
105.35	0.274±0.018	164.84	0.006±0.009
114.88	0.124±0.015	172.45	0.007±0.010
123.99	0.066±0.012	180.00	-0.026±0.016

may be floated independently within the stated systematic error. For each of Tables II–IV, the target polarization was maintained while changing the pion channel energy. The data in each of these tables should only be floated as a group.

The errors shown in the figures and tables reflect the statistical uncertainty plus that arising from the beam counting normalization correction.

The largest contribution to the systematic error arises from extracting the polarization using fits to the 139 MeV π^+ data of Sevier *et al.* The χ^2_ν obtained are of order 0.9–1.1, indicating that the shapes of these two data sets are certainly compatible. The total systematic error is thus the sum in quadrature of the systematic error quoted by Sevier *et al.* (1.6%) and the statistical error in the fit (1.4–2.3%), for a total estimated error of 2.8%. The calculation of the polarization for the π^- data explicitly required the dynamic NMR areas and thus has an additional error contribution

TABLE III. Measured analyzing power between 139 and 267 MeV π^+ . This is the second group of data taken at the same target polarization. These data should not be floated independently. The overall systematic error is 3%.

θ_c^π	$A_y(\theta) \pm \delta A_y(\text{stat})$	θ_c^π	$A_y(\theta) \pm \delta A_y(\text{stat})$
139.5 MeV π^+		169.0 MeV π^+	
72.86	0.454±0.020	62.50	0.390±0.043
83.76	0.451±0.012	73.92	0.425±0.021
94.22	0.349±0.009	84.87	0.446±0.018
104.24	0.252±0.008	95.33	0.370±0.016
113.83	0.151±0.007	105.32	0.271±0.015
123.03	0.102±0.009	114.85	0.141±0.014
131.87	0.061±0.008	123.96	0.105±0.018
140.39	0.035±0.006	132.69	0.021±0.017
148.64	0.030±0.006	141.09	0.034±0.012
156.67	0.005±0.006	149.21	0.006±0.012
172.30	-0.011±0.022	157.11	-0.013±0.013
180.00	-0.009±0.012	164.83	0.008±0.017
		172.45	-0.019±0.016
180.0 MeV π^+		193.2 MeV π^+	
62.85	0.363±0.016	51.29	0.317±0.050
74.30	0.437±0.010	63.26	0.363±0.013
85.26	0.461±0.009	74.75	0.439±0.010
95.73	0.392±0.008	85.73	0.462±0.010
105.70	0.278±0.008	96.19	0.406±0.010
115.21	0.140±0.007	106.14	0.262±0.009
124.29	0.079±0.009	115.62	0.138±0.010
132.98	0.038±0.009	124.67	0.067±0.011
141.34	-0.004±0.006	133.32	0.035±0.013
149.42	-0.007±0.006	141.63	-0.002±0.009
157.26	-0.002±0.007	149.65	-0.021±0.008
164.94	-0.007±0.007	157.44	-0.016±0.009
172.50	0.002±0.008	165.06	0.000±0.009
180.00	-0.009±0.014	172.56	0.012±0.010
		180.00	-0.002±0.011
218.0 MeV π^+		241.0 MeV π^+	
51.97	0.227±0.034	52.59	0.248±0.030
64.04	0.350±0.015	64.74	0.318±0.011
75.59	0.410±0.012	76.34	0.419±0.011
86.59	0.453±0.019	87.37	0.452±0.013
97.05	0.378±0.013	97.82	0.408±0.013
106.97	0.250±0.013	107.72	0.255±0.013
116.40	0.133±0.012	117.10	0.091±0.012
125.38	0.042±0.016	126.01	0.045±0.015
133.95	-0.015±0.014	134.50	-0.038±0.014
142.16	-0.013±0.010	142.64	-0.043±0.011
150.09	-0.038±0.011	150.47	-0.030±0.025
157.77	0.004±0.011	158.06	-0.021±0.015
165.28	-0.002±0.014	165.48	-0.027±0.016
172.67	0.003±0.013	172.77	0.002±0.013
180.00	0.010±0.017	180.00	0.004±0.016
267.0 MeV π^+		267.0 MeV π^+ (continued)	
53.27	0.197±0.016	135.12	-0.056±0.017
65.52	0.279±0.010	143.16	-0.055±0.013
77.18	0.396±0.011	150.89	-0.035±0.018
88.23	0.444±0.014	158.38	-0.051±0.015
98.67	0.415±0.015	165.69	-0.030±0.016
108.54	0.218±0.016	172.88	-0.031±0.018
117.86	0.073±0.015	180.00	-0.017±0.021
126.70	-0.011±0.020		

TABLE IV. Measured analyzing power at 193 and 241 MeV π^- . This is the third group of data taken at the same target polarization. The data at these two energies should not be floated independently. The overall systematic error is 3%.

193.2 MeV π^-		240.9 MeV π^-	
θ_c^π	$A_y(\theta) \pm \delta A_y(\text{stat})$	θ_c^π	$A_y(\theta) \pm \delta A_y(\text{stat})$
51.29	-0.277±0.095	64.74	-0.364 ± 0.017
63.26	-0.172±0.023	76.34	-0.350 ± 0.016
74.75	-0.158±0.017	87.37	-0.254 ± 0.017
85.73	-0.125±0.024	97.82	-0.156 ± 0.018
96.19	-0.155±0.017	107.72	-0.078 ± 0.018
106.14	-0.180±0.023	117.10	-0.035 ± 0.022
115.62	-0.185±0.020	126.01	0.020 ± 0.184
124.67	-0.408±0.175	134.50	-0.005 ± 0.042
133.32	-0.195±0.059	142.64	-0.020 ± 0.017
141.63	-0.114±0.017	150.47	-0.031 ± 0.014
149.65	-0.107±0.014	158.06	-0.017 ± 0.013
157.44	-0.057±0.012	165.48	-0.018 ± 0.012
165.06	-0.030±0.012	172.77	0.000 ± 0.016
172.56	0.001±0.015	180.00	-0.001 ± 0.027

from the extraction of these areas (0.8%). To simplify the analysis this error has been incorporated in the statistical error of these data. In summary, because of the unique data collection technique, an optimal analysis of these data should float only the *overall* polarization correction within the 2.8% error limits but *not* allow for an energy-by-energy systematic error.

VI. DISCUSSION

In addition to the 139 MeV π^+p data by Seviour *et al.*, there exist a total of six analyzing power measurements at incident energies comparable to the energies of this experiment. As expected, the 166 MeV and the 263 MeV πp data by Seviour *et al.* [9] agree very well with the new data, as shown in Fig. 3. The E560 data at 169 MeV π^+ are systematically lower than the forward angle data of Amsler *et al.* [12]. Raue *et al.* [11] recently reported three points at 165 MeV π^+p , only two (123.5°_{c.m.} and 142.8°_{c.m.}) of which overlap with the angular range of the E560 data, and they are in good agreement. The forward angle π^+ data at 240 MeV from the same group do show some discrepancies with the E560 data.

The data at 238 MeV published by Alder *et al.* [10] are the only overlapping data in the π^- reaction channel. Their results differ in shape as well as in magnitude from those obtained in the present experiment and hence the differences cannot be simply attributed to incorrect measurement of the target polarization or of the beam normalization.

A. Comparison to the phase shift analysis

A direct comparison of all the present data (π^+ and π^-) to the PWA of the Karlsruhe-Helsinki group (KH80) [3] and the more recently updated results from the VPI group (SM95) [18] results in a χ^2_ν of 3.0 (KH80) and 1.15 (SM95). Only statistical errors were considered. In order to make a comparison which is completely decoupled from the data of

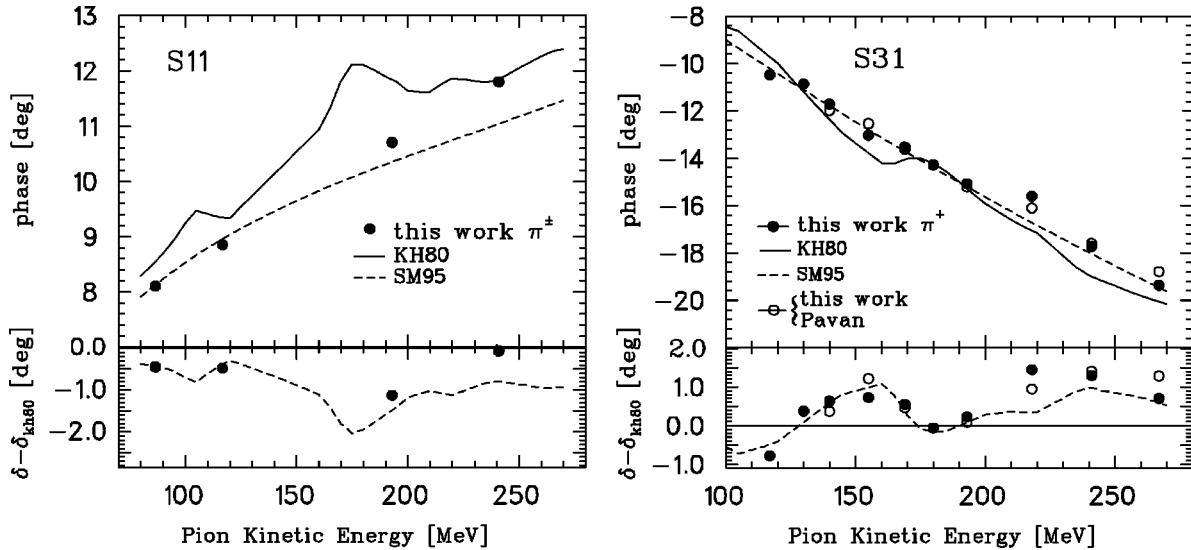


FIG. 5. The PHASAN-predicted phases for the partial waves S_{11} and S_{31} . The top part of the graphs show the phases for SM95 (dashed line), KH80 (solid line), and the new data set. The bottom graphs magnify the phase changes by plotting the new phases minus the KH80 values. For the S_{31} phase, the results of the simultaneous fit of the new data and those of Pavan [19] are also shown.

Sevior *et al.*, whose data are part of the SM95 database, the overall polarization calibration of the E560 data was floated to obtain a best fit. The total χ^2_ν of all the E560 data compared to these two PWA's now reduces to 1.10 (2.47) for SM95 (KH80). The largest differences between the data and the KH80 predictions arise in the π^- channel.

The present data were included in a novel PWA by Timmermans [4] (LG97). In this multienergy analysis, the overall polarization calibrations for π^+p and π^-p were independently floated. The PWA predicted a polarization correction of 0.993 (0.997) for π^-p (π^+p), resulting in overall χ^2_ν of 1.25 (0.97).

B. Single-energy analysis

The effect of the new A_y data on the partial-wave amplitudes was investigated using the the Karlsruhe PHASAN program (described in [3]), which allows a simultaneous single-energy fit of several πp observables. The program assumes isospin invariance and unitarity and uses forward amplitudes derived by Höhler [2], which are based on previous total cross-section data. The E560 data were fit independently and also in combination with the recent differential cross-section measurements by Pavan [19] at those energies where the experiments overlapped. Only S and P waves were varied. The higher partial waves and starting values for S and P waves were taken from the KA84 solution. KA84 is essentially an energy-smoothed version of KH80. To calculate the isospin-1/2 phases, the π^+ and π^- data were fitted simultaneously. Fitting the π^- data alone could have allowed the program to modify the isospin-3/2 phases in a manner inconsistent with the π^+ data.

The resulting (L_{2J2J}) S_{11} and S_{31} phases and those of SM95 and KH80 are plotted in Fig. 5. The bottom graphs show the same phases subtracted from the KH80 phases to emphasize the differences. Although the starting phases were those of KA84, the final phases favor those of the SM95 solutions. Results for the P waves show relatively smaller

differences and depended strongly on whether the Pavan data were left in or out of the fits.

The figures compare hadronic amplitudes. It should, however, be noted that the Karlsruhe-Helsinki analysis and the Virginia analysis use different methods of electromagnetic corrections in extracting the hadronic amplitudes from the experimental observables.

Similar simultaneous fits of the present A_y data with other existing differential cross-section measurements [20–24] showed that all could be accommodated. This lack of discrimination is attributed to the dominance of a single resonant partial wave in the differential cross sections at these energies, whereas the analyzing power, an interference of amplitudes, is equally sensitive to the smaller partial waves. Note that the recent data of Raue *et al.* [11], which disagree with the E560 data at 240 MeV π^+ by many standard deviations, could not be fitted well. When included, the resulting χ^2_ν was 15.87, which is to be contrasted to 0.75 for the E560 data.

VII. SUMMARY

We have presented πp elastic analyzing powers at 10 π^+ and 4 π^- energies. Because of persistent target NMR problems, the data have been normalized to those of Sevior *et al.* at 139 MeV π^+ . The technique of varying the beam energy while maintaining the target polarization produced a strongly coupled set of data spanning the Δ resonance. Furthermore, the 360° acceptance of the CHAOS spectrometer eliminated the systematic error normally associated with counting of the incident pion beam. Preliminary phase shift analysis show that the data are consistent with the new PWA of Timmermans [4] and that the data favor the hadronic S_{11} and S_{31} phase shifts of the Virginia group SM95 [18] solution. The data are now part of the recently updated SP98 [25] analysis. Data reduction and analysis of the low-energy π^- data, collected with a fully functional polarized target, are presently underway.

ACKNOWLEDGMENTS

We wish to thank TRIUMF for the support given to the experiment both on a technical level as well as financially. In particular we wish to single out the efforts of the TRIUMF polarized target group. We also gratefully acknowledge fi-

nancial support which made this work possible, from the National Science and Engineering Research Council of Canada, the Istituto Nazionale di Fisica Nucleare of Italy, the Australian Research Council, the U.S. Department of Energy, the VW-Stiftung, and the California State University Sacramento Foundation.

-
- [1] T. P. Cheng and R. Dashen, *Phys. Rev. Lett.* **26**, 594 (1971).
 [2] G. Höhler, in *Pion Nucleon Scattering*, edited by H. Schopper, Landolt-Börnstein, New Series, Group X, Vol. I/9b2 (Springer Verlag, Berlin, 1983).
 [3] R. Koch and E. Pietarinen, *Nucl. Phys.* **A336**, 331 (1980).
 [4] R. Timmermans, in *Proceedings of the VIIth International Symposium on Meson-Nucleon Physics*, Vancouver, Canada edited by D. Drechsel, G. Höhler, W. Kluge, H. Leutwyler, B. M. K. Nefkens, and H.-M. Staudenmaier [*πN Newsletter* **13**, 80 (1997)].
 [5] M. Pavan and R. A. Arndt, in [4], p 165.
 [6] W. R. Gibbs, Li Ai, and W. B. Kaufmann, *Phys. Rev. Lett.* **74**, 3740 (1995).
 [7] E. Matsinos, "Isospin Violation in the πN System at Low Energies," Report No. ETHZ-IPP PR-97-02, 1997.
 [8] R. Wieser *et al.*, *Phys. Rev. C* **54**, 1930 (1996).
 [9] M. E. Sevier *et al.*, *Phys. Rev. C* **40**, 2780 (1989).
 [10] J. Alder *et al.*, *Phys. Rev. D* **27**, 1040 (1983).
 [11] B. Raue *et al.*, *Phys. Rev. C* **53**, 1005 (1996).
 [12] C. Amsler, L. Dubal, G. H. Eaton, R. Frosch, S. Mango, F. Pozar, and U. Rohrer, *Lett. Nuovo Cimento* **15**, 209 (1976).
 [13] G. R. Smith *et al.*, *Nucl. Instrum. Methods Phys. Res. A* **362**, 345 (1995).
 [14] P. P. J. Delheij and I. Sekachev, *Nucl. Instrum. Methods Phys. Res. A* **356**, 56 (1995).
 [15] G. J. Hofman, J. T. Brack, P. A. Amaudruz, and G. R. Smith, *Nucl. Instrum. Methods Phys. Res. A* **325**, 384 (1993).
 [16] K. J. Raywood, S. J. McFarland, P. A. Amaudruz, G. R. Smith, and M. E. Sevier, *Nucl. Instrum. Methods Phys. Res. A* **357**, 296 (1995).
 [17] F. Bonutti, S. Buttazzoni, P. Camerini, N. Grion, and R. Rui, *Nucl. Instrum. Methods Phys. Res. A* **350**, 136 (1994).
 [18] R. A. Arndt, I. Strakovsky, R. Workman, and M. Pavan, *Phys. Rev. C* **52**, 2120 (1995).
 [19] M. Pavan, Ph.D. thesis, The University of British Columbia, 1995.
 [20] J. T. Brack *et al.*, *Phys. Rev. C* **34**, 1771 (1986).
 [21] J. T. Brack *et al.*, *Phys. Rev. C* **38**, 2427 (1988).
 [22] J. T. Brack *et al.*, *Phys. Rev. C* **41**, 2202 (1990).
 [23] J. T. Brack *et al.*, *Phys. Rev. C* **51**, 929 (1995).
 [24] P. J. Bussey, J. R. Carter, D. R. Dance, D. V. Bugg, A. A. Carter, and A. M. Smith, *Nucl. Phys.* **B58**, 363 (1973).
 [25] R. A. Arndt, I. I. Strakovsky, and R. L. Workman, *Scattering Analysis Interactive Dial-In (SAID)*, available at <http://clsaid.phys.vt.edu/~CAPS>